Rapid Communications | Editors' Suggestion

High-field quantum disordered state in α-$RuCl_3$: Spin flips, bound states, and multiparticle continuum

A. Sahasrabudhe,[1] D. A. S. Kaib,[2] S. Reschke,[3] R. German,[1] T. C. Koethe,[1] J. Buhot,[4] D. Kamenskyi,[4] C. Hickey,[5] P. Becker,[6] V. Tsurkan,[3,7] A. Loidl,[3] S. H. Do,[8] K. Y. Choi,[8] M. Grüninger,[1] S. M. Winter,[2] Zhe Wang,[1,9] R. Valentí,[2] and P. H. M. van Loosdrecht[1]

[1]*Institute of Physics II, University of Cologne, 50937 Cologne, Germany*
[2]*Institut für Theoretische Physik, Goethe-Universität Frankfurt, 60438 Frankfurt am Main, Germany*
[3]*Experimental Physics V, Center for Electronic Correlations and Magnetism, University of Augsburg, 86159 Augsburg, Germany*
[4]*High Field Magnet Laboratory, EMFL, Radboud University, 6525 ED Nijmegen, The Netherlands*
[5]*Institute for Theoretical Physics, University of Cologne, 50937 Cologne, Germany*
[6]*Institute for Geology and Mineralogy, University of Cologne, 50674 Cologne, Germany*
[7]*Institute of Applied Physics, MD2028 Chisinau, Republic of Moldova*
[8]*Department of Physics, Chung-Ang University, Seoul 06974, Republic of Korea*
[9]*Institute of Radiation Physics, Helmholtz Zentrum Dresden-Rossendorf, 01328 Dresden, Germany*

(Received 30 August 2019; accepted 25 March 2020; published 24 April 2020)

Layered α-$RuCl_3$ has been discussed as a proximate Kitaev spin-liquid compound. Raman and terahertz spectroscopy of magnetic excitations confirms that the low-temperature antiferromagnetic ordered phase features a broad Raman continuum, together with two magnonlike excitations at 2.7 and 3.6 meV, respectively. The continuum strength is maximized as long-range order is suppressed by an external magnetic field. The state above the field-induced quantum phase transition around 7.5 T is characterized by a gapped multiparticle continuum out of which a two-particle bound state emerges, together with a well-defined single-particle excitation at lower energy. Exact diagonalization calculations demonstrate that Kitaev and off-diagonal exchange terms in the Fleury-Loudon operator give rise to a pronounced intensity of these features in the Raman spectra. Our Rapid Communication firmly establishes the partially polarized quantum disordered character of the high-field phase.

DOI: 10.1103/PhysRevB.101.140410

Integrable models are of great interest, as the relevant physics of such models can be obtained in an exact sense. A canonical example is the fractionalization of excitations in the one-dimensional spin-1/2 Heisenberg-Ising chain. While a single spin flip changes the total spin by 1, the elementary excitations of this model are spinons, which carry a fractional quantum number of spin 1/2 [1]. Spin fractionalization also occurs in two-dimensional integrable models, with a particularly prominent example being the spin-1/2 Kitaev honeycomb model composed of bond-dependent Ising interactions [2]. Its exact solution results in an exotic quantum spin-liquid (QSL) ground state, where spin-flip excitations fractionalize into gapless Majorana fermions and gapped flux excitations [2–6].

Candidate materials for realizing the fascinating physics of the Kitaev model feature Ir^{4+} or Ru^{3+} ions with spin-orbit entangled $j = 1/2$ moments [7]. The presence of dominant ferromagnetic Kitaev interactions is well established in A_2IrO_3 (A = Na or Li) and α-$RuCl_3$ [3–6,8]. However, they appear simultaneously with subleading isotropic Heisenberg and anisotropic off-diagonal exchange interactions [3–6], resulting in long-range order below a finite temperature T_N, hampering experimental observation of the Kitaev QSL.

There remain, though, promising alternate avenues to observing the sought-after QSL physics. On the one hand, by going to elevated temperatures above T_N, various spectroscopic studies of spin dynamics have found features reminiscent of the Kitaev QSL in α-$RuCl_3$ [9–14]. On the other hand, one may suppress the long-range order by tuning external parameters [12,15–30], e.g., magnetic field, in order to hopefully detect the QSL as a field-induced phase, before reaching the partially polarized quantum disordered state (QDS), that is smoothly connected to the fully field-polarized limit [due to the lack of SU(2) symmetry, the polarized state is only approached asymptotically with increasing field strength].

In α-$RuCl_3$, a variety of experimental studies have reported a single field-induced quantum phase transition with an in-plane critical field of $B_c = 6$–8 T [12,16–20,22–26]. The nature of the subsequent field-induced phase has been under strong scrutiny, with conflicting reports over whether it is gapped or gapless and whether it is the sought-after QSL or the partially field-polarized state [12,16–26]. We also note that in some more recent studies additional field-induced phase transitions were reported [27,28], within the narrow field range 6–10 T. An intermediate region with quantized thermal Hall conductivity has further been reported [29].

Raman scattering has been suggested as being particularly powerful in revealing signatures of spin fractionalization of the Kitaev QSL as it naturally probes the emergent Majorana fermion excitations [31]. In α-$RuCl_3$, the experimentally

observed broad Raman continuum at zero field was taken as evidence for spin fractionalization [9,31], while in particular its temperature dependence was claimed to reflect the character of fermionic excitations [9,13,32]. The Raman response of the possible field-induced phases so far remained unexplored.

In this Rapid Communication, we study the magnetic excitations of α-$RuCl_3$ as a function of in-plane magnetic field up to 33 T using Raman and terahertz spectroscopy. The Raman continuum exhibits maximum intensity as soon as the long-range zig-zag (ZZ) antiferromagnetic order is suppressed at $B_c = 7.5$ T. In the high-field limit, we observe a gapped continuum of multiparticle excitations. Below this continuum, both Raman and terahertz spectroscopy reveal a two-particle bound state as well as a sharp single-particle excitation. These features are most clearly resolved in the high-field regime above 15 T, yielding a clear picture of the properties of the high-field phase. At intermediate fields near B_c, the features start to overlap in energy, which partially explains previous difficulties in understanding the field-induced phase. The access to the high-field limit further allows us to resolve a long-standing controversy regarding anomalously steep slopes [12,21,23] of the excitation modes at intermediate fields. Our numerical calculations essentially capture the field-dependent features, and highlight that the presence of dominant Kitaev exchange and off-diagonal interactions can explain the surprising strength of one-magnon Raman scattering that usually is very weak in conventional antiferromagnets.

High-quality α-$RuCl_3$ crystals for our Rapid Communication were prepared by vacuum sublimation. They exhibit a sharp magnetic phase transition at $T_N = 6.5$ K [11,33]. High-field Raman back-scattering and terahertz-transmission experiments on samples from Augsburg [33,34] and Seoul [11,12] were performed in Bitter magnets for in-plane fields up to 30 and 33 T, respectively, at a cryostat base temperature of 1.7 and 2 K. Both experiments were carried out in a Voigt geometry, i.e., $\mathbf{B} \perp \mathbf{k}$, with the incident wave vector $\mathbf{k}$ perpendicular to the sample's hexagonal *ab* plane. The field was oriented nearly perpendicular (within 10°) to the nearest-neighbor Ru-Ru bonds, while the in-plane field orientation was not determined for the terahertz measurements. For Raman spectroscopy, circularly polarized (*L* for left and *R* for right) light with a wavelength of 532 nm was focused into a spot of about 2 μm on freshly cleaved samples. Terahertz transmission spectra were recorded on samples with a typical *ab* surface of 3×3 mm^2 and thickness of 1 mm using a Fourier-transform spectrometer Bruker IFS-113v, with a mercury lamp as source and a silicon bolometer as detector.

To minimize heating effects due to the incident beam, we applied a very low laser power of 10 μW for the Raman spectroscopy of the low-field ordered phase. Figure 1(a) presents the Raman spectra in the *LR* circularly polarized channel in magnetic fields of up to 9 T. While the zero-field Raman spectrum is dominated by a broad scattering continuum in accordance with previous Raman studies [9,13,35], we can also discern two peaks of magnetic excitations in the low-energy regime at 2.7 and 3.6 meV, respectively, as indicated by the arrows in Fig. 1(a) and its inset, which shift systematically to lower energies with increasing magnetic

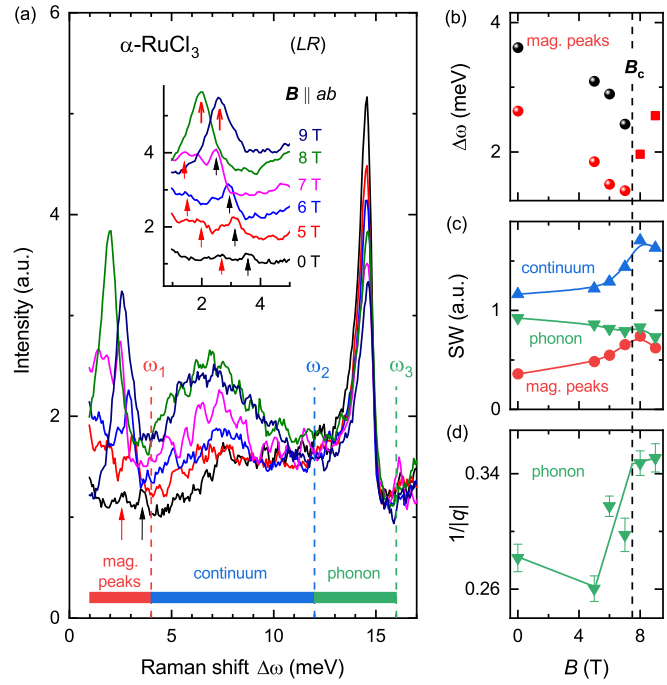

FIG. 1. (a) Circularly polarized (*LR*) Raman spectra recorded at 1.7 K with low incident laser power of 10 μW in fields up to 9 T. Inset: Magnetic excitations are resolved at low energies, as indicated by the arrows. The spectra of different fields are shifted upward by a constant for clarity. (b) Energy transfer of the magnetic excitations in (a) is shown as a function of field. (c) Spectral weight for different frequency ranges, as indicated by the dashed lines in (a). (d) Fano parameter $1/|q|$ for the 15-meV phonon. The solid line is a guide to the eye. The dashed line in (b)–(d) indicates the critical field $B_c = 7.5$ T.

field up to 7 T [Fig. 1(b)]. These two modes, in energy and field dependence comparable to those reported in previous neutron-scattering [10], electron-spin resonance [23], and terahertz spectroscopic studies [12,36–38], correspond to the single-magnon excitations at the Γ point of the ZZ ordered state. While this observation clearly indicates that our sample temperature stayed well below T_N, we found that increasing the laser power to 100 μW is sufficient to erase these two modes from the Raman spectra [see Fig. 2(a)], which explains the absence of these modes in the previous Raman studies. Above $B_c = 7.5$ T, only a single peak dominates the low-energy Raman response [Fig. 1(a)]. In particular, for 8 T, where evidence for a separate intermediate phase has been reported in recent thermodynamic measurements [29,30], we find a sharp peak $m_{1\alpha}$ at 2 meV in the Raman spectrum. Consistent with reported terahertz results [12,23], this mode hardens continuously in higher fields above B_c (Fig. 2), without any obvious features indicating a second field-induced phase transition.

At higher energies, the zero-field Raman response presents a set of phonon modes, in accordance with previous Raman studies [9,13,35]. The lowest phonon at 15 meV exhibits an asymmetric Fano line shape which reflects interference with an underlying continuum. The line-shape asymmetry quantified by the Fano parameter q is represented as $1/|q|$

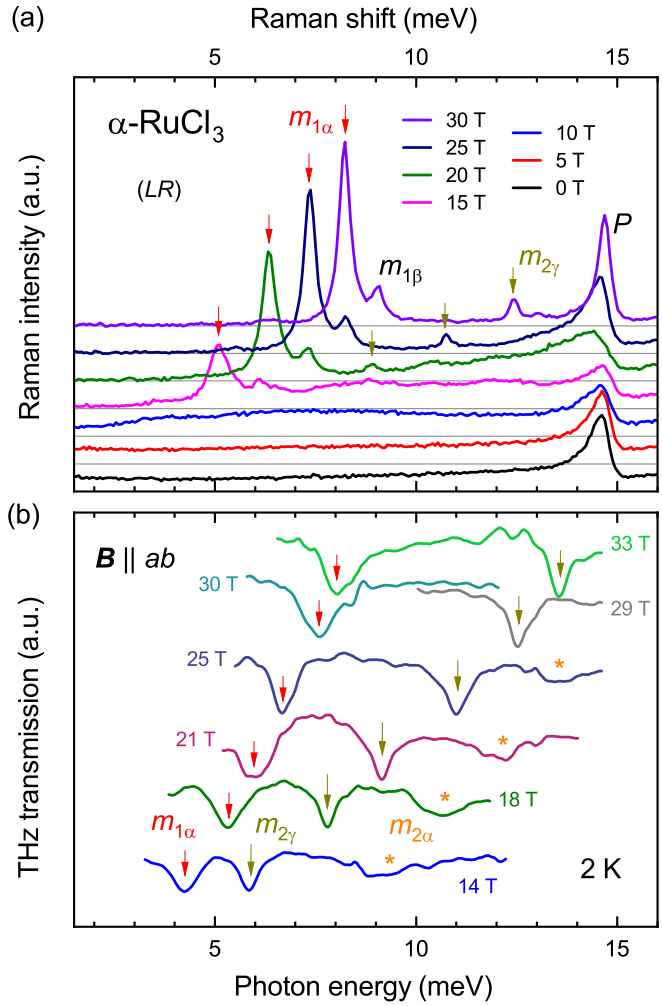

FIG. 2. High-field (a) 100-μW *LR*-Raman and (b) unpolarized terahertz-transmission spectra. A variety of field-dependent features are indicated (see text for details). *P* denotes phonon.

in Fig. 1(d). Approaching the critical field from below, $1/|q|$ displays an abrupt increase, indicating that the interference is strongly enhanced at B_c. This is primarily due to the increase of the scattering strength of the continuum, and also indicates that the 15-meV phonon modulating the Ru-Ru bond [35] is strongly coupled to the magnetic degrees of freedom. For higher fields, the continuum moves to higher energy [see Fig. 2(a)]. This leads to a further increase of the asymmetry reaching a maximum around 20 T. Above these fields the asymmetry decreases again as the scattering intensity in the vicinity of the phonon energy decreases until the line shape becomes nearly symmetric at the highest field measured.

In addition to the high-energy phonons and the low-energy magnonlike excitations, the zero-field spectrum is marked by an extended continuum [8,9,11–14,35], that shows a broad intensity maximum in the midenergy region between 4 and 12 meV. Figure 1(c) displays the integrated spectral weight for three different energy regions [indicated by dashed lines in Fig. 1(a)] as a function of field strength. While the spectral weight of the 15-meV phonon is reduced at higher fields, both the low-energy excitations and the midfrequency continuum are clearly enhanced upon approaching the field-induced quantum phase transition at $B_c = 7.5$ T.

To obtain a comprehensive picture of the field-induced phase above B_c, we carried out both Raman and terahertz spectroscopic measurements, the results of which are presented in Fig. 2. With an increased laser power of 100 μW, the signal-to-noise ratio of the Raman spectra is improved, allowing us to resolve the high-field features. At the same time, due to additional heating effects, the low-energy magnons that were present in Fig. 1(a) cannot be resolved here, and the $m_{1\alpha}$ mode seen sharply at 8 T is also weakened, but becomes stronger and easily recognized above 10 T. At 15 T, the $m_{1\alpha}$ mode is observed at 5.1 meV and accompanied by a satellite peak $m_{1\beta}$ at 6.1 meV, both of which become sharper and shift to higher energy with increasing fields. While the field dependence of the $m_{1\alpha}$ mode is consistently seen by the terahertz spectroscopy data [Fig. 2(b)], the satellite peak is hardly resolvable. It is worth noting that the $m_{1\alpha}$ peak position in the terahertz spectra is located slightly lower, about 0.6 meV, than in the corresponding Raman spectra, which comparable to in-plane anisotropy [38] can be due to uncertainty in our in-plane field orientation.

Another sharp feature in the Raman spectra is the observation of mode $m_{2\gamma}$ at higher energy, which is located at 12.4 meV at 30 T and which shows a steeper increase in energy with field, as compared with the dominant $m_{1\alpha}$ mode. Consistent energy and field dependence is also found in the terahertz spectra, but the relative intensity $I_{m_{2\gamma}}/I_{m_{1\alpha}}$ is much stronger in terahertz [Fig. 2(b)].

A unique feature present in the high-field Raman response is the underlying continuum of excitations. In contrast to the spectra below B_c, one can clearly see a gap opening at B_c with the lower bound of the continuum shifting towards higher energy upon increasing field. For instance, at 15 T, the spectral weight below 3 meV is almost fully depleted, just below the $m_{1\alpha}$ mode, signaling a gap opening. The lower bound of the continuum shifts with a similarly steep slope as $m_{2\gamma}$ to higher energies, approximately twice that of $m_{1\alpha}$. These features are better illustrated in the color plot of the Raman intensity in Fig. 3(a). Usually, a featureless continuum is rare to resolve in terahertz spectroscopy, but as marked by the asterisk in Fig. 2(b) we can track a broad transmission minimum $m_{2\alpha}$ as a function of field, in agreement with that of the Raman continuum [Fig. 3(a)]. Thus, the terahertz $m_{2\alpha}$ band captures the broad maximum of the underlying continuum with its strong field-dependence.

The fact that the modes $m_{1\alpha}$ and $m_{2\gamma}$ are observed both in the terahertz response and in Raman aids significantly in their identification. Based on comparison with previous linear-polarized lower-field terahertz studies [12,21], we identify the $m_{1\alpha}$ mode as a single-particle excitation expected in the QDS, which is well described by linear spin-wave theory as a single magnon only at sufficiently high fields. Going to stronger fields we observe that the higher-energy continuum exhibits a somewhat broad maximum $m_{2\alpha}$, which has approximately twice the energy of $m_{1\alpha}$, i.e., $m_{2\alpha} = 2m_{1\alpha}$ [Fig. 3(a)]. This identifies the lower band near $m_{2\alpha}$ of the multiparticle continuum to consist predominantly of two-particle excitations. However, an additional observation enabled by going to higher fields is the clear separation of an apparent

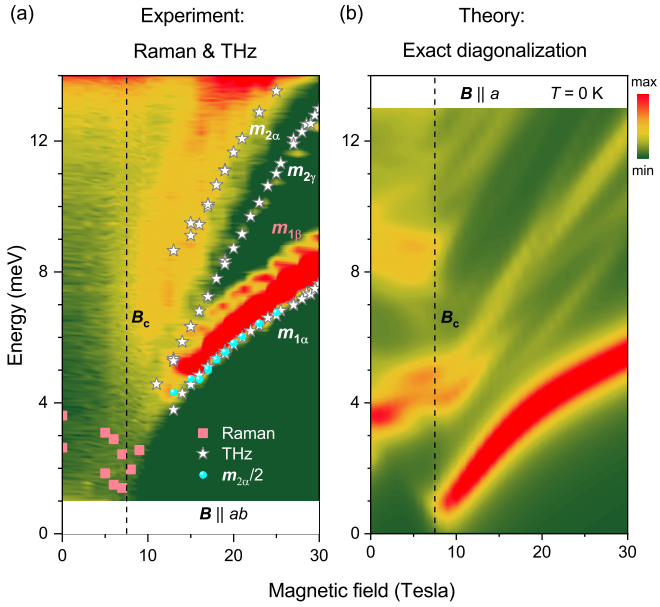

FIG. 3. (a) Contour plot of experimental 100-μW Raman intensity of α-$RuCl_3$ as a function of in-plane field [from Fig. 2(a)]. Peak positions obtained in the low-field 10-μW Raman spectra ($B \leqslant 8$ T) [Fig. 1(b)] and in the high-field terahertz spectra ($B \geqslant 10$ T) [Fig. 2(b)] are shown by symbols for comparison. (b) Theoretical $T = 0$ Raman response within the Fleury-Loudon approximation [39] of a C_3-broken model for $\mathbf{B} \parallel a$ assuming $g_{ab} = 2.3$ (see Supplemental Material [41]).

two-particle bound state $m_{2\gamma}$ slightly below the multiparticle continuum and well above $m_{1\alpha}$. The two-particle nature of $m_{2\gamma}$ is consistent with the polarization dependence in terahertz [12,21]. Finally, the field dependence of the satellite peak $m_{1\beta}$ follows that of $m_{1\alpha}$ with a nearly field-independent energy difference of about 1 meV, which suggests that $m_{1\beta}$ could be due to multiparticle scattering or interlayer coupling. We note that a recent neutron-scattering study revealed out-of-plane dispersion of the single-particle excitations with a bandwidth of around 1 meV [30].

The observation and in particular the strength of the single-particle mode $m_{1\alpha}$ in Raman spectroscopy may appear surprising at first. Typically, via the so-called Fleury-Loudon scattering processes [39], the magnetic Raman response is dominated by two-magnon excitations. Single-magnon scattering in general is active in the presence of spin-orbit coupling but usually is much weaker, as exemplified by Raman data on the Heisenberg compounds Sr_2IrO_4 and $Sr_3Ir_2O_7$ with strong spin-orbit coupling [40]. To explain the pronounced Raman intensity of $m_{1\alpha}$, we consider the infinite-field polarized limit $|\mathbf{B}| \to \infty$, in which case the exact ground state is an eigenstate of S^{μ}_{tot}, with μ being the direction of $\mathbf{g} \cdot \mathbf{B}$. In this case, terms in the Fleury-Loudon scattering operator like $S^{\mu}_i S^{\nu}_j$, with $\mu \neq \nu$, may create single spin-flip ($|\Delta S| = 1$) excitations (which correspond to single magnons in the polarized limit). Indeed, such terms naturally arise in the presence of Kitaev and off-diagonal exchanges (see Supplemental Material [41]), making α-$RuCl_3$ a striking example of this unusual Raman response.

An important quantity of interest is the slope of the excitation energy of the $m_{1\alpha}$ mode as a function of field, $g^* \equiv \frac{dE_{m_{1\alpha}}}{\mu_B dB}$. In the large-field limit, one expects this to approach $g^*|_{B\to\infty} = g_{ab}|\Delta S|$. Since the intrinsic Landé in-plane g value is constrained to $2 \leqslant g_{ab} \leqslant 2.8$ [4,42,43], the asymptotic slope provides information regarding g_{ab} and the character of the excitation. In this regard, the reported slopes of $g^* \gtrsim 8$ for measurements near the critical field ($B \gtrsim B_c$) [12,23] have been discussed as evidence for either fractionalized excitations of a field-induced QSL state, an enormous in-plane g value $g_{ab} \approx 10$, or an apparent multiparticle bound-state character of mode $m_{1\alpha}$. However, the direct comparison of the measured slopes with the polarized limit has two major caveats.

(i) Level repulsion between $m_{1\alpha}$ and the continuum may significantly increase the slope in the vicinity of B_c.

(ii) Since the anisotropic couplings produce an effective easy-plane anisotropy in the QDS [44,45], the slope of the single-particle excitation is expected to approach g_{ab} only asymptotically (see Ref. [46]).

Indeed we find that g^* drops from 8 at around 10 T [12] continuously to about 3 at 30 T. By analyzing the data over the full field range we extract an asymptotic $g^*|_{B\to\infty} = 2.51 \pm 0.18$ (see Supplemental Material [41]) which confirms $m_{1\alpha}$ as the mode that evolves into the $|\Delta S| = 1$ spin-flip excitation in the infinite-field limit.

To complement the experimental results, we perform exact diagonalization (ED) calculations of suitable realistic models on a 24-site cluster (see Supplemental Material [41]), with parameters based on *ab initio* studies [43,47–50]. The Raman intensity $I(\omega) = \int dt\, e^{-i\omega t} \langle \mathcal{F}(t)\mathcal{F}(0)\rangle$ is evaluated using the Fleury-Loudon approach [39], with the scattering operator $\mathcal{F} \propto \sum_{ij} \mathbf{S}_i \cdot \hat{\mathbf{J}}_{ij} \cdot \mathbf{S}_j\, (\boldsymbol{\delta}_{ij} \cdot \mathbf{E}_{\text{in}})(\boldsymbol{\delta}_{ij} \cdot \mathbf{E}^*_{\text{out}})$ where $\hat{\mathbf{J}}_{ij}$ contains the generic couplings between $\mathbf{S}_i$ and $\mathbf{S}_j$, $\boldsymbol{\delta}_{ij}$ is the distance vector between sites i and j, and $\mathbf{E}_{\text{in}}$ ($\mathbf{E}_{\text{out}}$) is the direction of the electric field of the incident (outgoing) light. Our ED study is found to reproduce the essential features of the Raman measurements: At low fields $B < B_c$, a continuum of excitations extending throughout a wide energy range. For $B > B_c$, the lower bound of the continuum quickly rises in energy, and a strong single-particle mode ($m_{1\alpha}$) emerges, becoming the most intense excitation at high field. The multiparticle continuum is also reproduced in ED; however, the existence of a distinct bound state ($m_{2\gamma}$) separate from the continuum is difficult to assess in ED, due to the discrete nature of the computed spectra on finite-size clusters. It should be noted that not all models capture the strong-field dependence of g^*. Figure 3(b) shows the results for an adjusted model which does capture this, namely, $(J_1, K_1^{x/y}, K_1^z, \Gamma_1, J_3) = (-0.5, -7.5, -5, 2.5, 0.5) \times 1.5$ meV. The employed breaking of C_3 symmetry ($K_1^x = K_1^y \neq K_1^z$) is motivated by *ab initio* calculations [47] for the $C2/m$ structure of α-$RuCl_3$ [16,51]. As observed in the experiment [Fig. 3(a)], a continuum extends throughout a wide energy range below B_c in the numerical results [Fig. 3(b)], while for $B > B_c$ the continuum rises in energy. Above B_c, a strong, sharp mode emerges at lowest energies, which shifts to higher energy and becomes the most intense excitation at high fields.

This mode follows the field-induced excitation-gap opening, corresponding to the observed $m_{1\alpha}$ mode in Fig. 3(a). We have further studied separately the contributions of the Heisenberg and the off-diagonal exchange terms (see Supplemental Material [41]), and confirmed that the Kitaev and the off-diagonal exchanges in $\mathcal{F}$ can explain the unusual strength of the single-particle excitation in the Raman response.

In conclusion, our Rapid Communication shows that the high-field phase in α-$RuCl_3$, which emerges through the suppression of antiferromagnetic order, is neither a quantum spin-liquid state nor a fully field-polarized state, but rather a quantum disordered state with partial field alignment of the spin-orbital moments. No clear evidence is found for an intermediate phase around 7.5 T in our experiments. The high-field phase is spectroscopically characterized by a strong and sharp single-particle excitation and a continuum of multiparticle nature, out of which a well-defined two-particle bound state emerges, best visible at higher fields. A comparison of experimental and exact diagonalization results clearly demonstrates the importance of Kitaev and off-diagonal interactions in α-$RuCl_3$. Based on the current Rapid Communication one expects similar high-field physics in other Kitaev candidate materials such as the iridates.

Note added in proof. Recently a second interesting study on high field Raman scattering in $RuCl_3$ appeared which is in line with the current observations [52].

We acknowledge helpful discussions with A. L. Chernyshev, J. Knolle, S. Trebst, and P. A. Maksimov. This work is partially supported by the German Research Foundation via Grant No. 277146847, CRC 1238 "Control and Dynamics of Quantum Materials"; Grant No. 107745057, TRR 180, "From Electronic Correlations to Functionality" (Subproject No. F5); and via Project No. VA117/15-1, "Probing the nature of excitations in spin-orbit-coupled materials from first principles." We acknowledge the support of the High Field Magnet Laboratory, member of the European Magnetic Field Laboratory.

[1] L. D. Faddeev and L. A. Takhtajan, Phys. Lett. A **85**, 375 (1981).
[2] A. Kitaev, Ann. Phys. (NY) **321**, 2 (2006).
[3] S. Trebst, arXiv:1701.07056v1.
[4] S. M. Winter, A. A. Tsirlin, M. Daghofer, J. van den Brink, Y. Singh, P. Gegenwart, and R. Valenti, J. Phys.: Condens. Matter **29**, 493002 (2017).
[5] M. Hermanns, I. Kimchi, and J. Knolle, Annu. Rev. Condens. Matter Phys. **9**, 17 (2018).
[6] H. Takagi, T. Takayama, G. Jackeli, G. Khaliullin, and S. E. Nagler, Nat. Rev. Phys. **1**, 264 (2019).
[7] G. Jackeli and G. Khaliullin, Phys. Rev. Lett. **102**, 017205 (2009).
[8] A. Banerjee, J. Yan, J. Knolle, C. A. Bridges, M. B. Stone, M. D. Lumsden, D. G. Mandrus, D. A. Tennant, R. Moessner, and S. E. Nagler, Science **356**, 1055 (2017).
[9] L. J. Sandilands, Y. Tian, K. W. Plumb, Y.-J. Kim, and K. S. Burch, Phys. Rev. Lett. **114**, 147201 (2015).
[10] A. Banerjee, C. A. Bridges, J.-Q. Yan, A. A. Aczel, L. Li, M. B. Stone, G. E. Granroth, M. D. Lumsden, Y. Yiu, J. Knolle *et al.*, Nat. Mater. **15**, 733 (2016).
[11] S.-H. Do, S.-Y. Park, J. Yoshitake, J. Nasu, Y. Motome, Y. S. Kwon, D. T. Adroja, D. J. Voneshen, K. Kim, T.-H. Jang *et al.*, Nat. Phys. **13**, 1079 (2017).
[12] Z. Wang, S. Reschke, D. Hüvonen, S.-H. Do, K.-Y. Choi, M. Gensch, U. Nagel, T. Rõom, and A. Loidl, Phys. Rev. Lett. **119**, 227202 (2017).
[13] Y. Wang, G. B. Osterhoudt, Y. Tian, P. Lampen-Kelley, A. Banerjee, T. Goldstein, J. Yan, J. Knolle, H. Ji, R. J. Cava *et al.*, npj Quantum Mater. **5**, 14 (2020).
[14] S. Reschke, V. Tsurkan, S.-H. Do, K.-Y. Choi, P. Lunkenheimer, Z. Wang, and A. Loidl, Phys. Rev. B **100**, 100403 (2019).
[15] Y. Kubota, H. Tanaka, T. Ono, Y. Narumi, and K. Kindo, Phys. Rev. B **91**, 094422 (2015).
[16] R. D. Johnson, S. C. Williams, A. A. Haghighirad, J. Singleton, V. Zapf, P. Manuel, I. I. Mazin, Y. Li, H. O. Jeschke, R. Valentí *et al.*, Phys. Rev. B **92**, 235119 (2015).
[17] I. A. Leahy, C. A. Pocs, P. E. Siegfried, D. Graf, S.-H. Do, K.-Y. Choi, B. Normand, and M. Lee, Phys. Rev. Lett. **118**, 187203 (2017).
[18] J. A. Sears, Y. Zhao, Z. Xu, J. W. Lynn, and Y.-J. Kim, Phys. Rev. B **95**, 180411(R) (2017).
[19] A. U. B. Wolter, L. T. Corredor, L. Janssen, K. Nenkov, S. Schönecker, S.-H. Do, K.-Y. Choi, R. Albrecht, J. Hunger, T. Doert *et al.*, Phys. Rev. B **96**, 041405(R) (2017).
[20] S.-H. Baek, S.-H. Do, K.-Y. Choi, Y. S. Kwon, A. U. B. Wolter, S. Nishimoto, J. van den Brink, and B. Büchner, Phys. Rev. Lett. **119**, 037201 (2017).
[21] S. M. Winter, K. Riedl, D. Kaib, R. Coldea, and R. Valentí, Phys. Rev. Lett. **120**, 077203 (2018).
[22] N. Janša, A. Zorko, M. Gomilšek, M. Pregelj, K. W. Krämer, D. Biner, A. Biffin, C. Rüegg, and M. Klanjšek, Nat. Phys. **14**, 786 (2018).
[23] A. N. Ponomaryov, E. Schulze, J. Wosnitza, P. Lampen-Kelley, A. Banerjee, J.-Q. Yan, C. A. Bridges, D. G. Mandrus, S. E. Nagler, A. K. Kolezhuk *et al.*, Phys. Rev. B **96**, 241107(R) (2017).
[24] J. Zheng, K. Ran, T. Li, J. Wang, P. Wang, B. Liu, Z.-X. Liu, B. Normand, J. Wen, and W. Yu, Phys. Rev. Lett. **119**, 227208 (2017).
[25] R. Hentrich, A. U. B. Wolter, X. Zotos, W. Brenig, D. Nowak, A. Isaeva, T. Doert, A. Banerjee, P. Lampen-Kelley, D. G. Mandrus *et al.*, Phys. Rev. Lett. **120**, 117204 (2018).
[26] A. Banerjee, P. Lampen-Kelley, J. Knolle, C. Balz, A. A. Aczel, B. Winn, Y. Liu, D. Pajerowski, J. Yan, C. A. Bridges, A. T. Savici *et al.*, npj Quantum Mater. **3**, 8 (2018).
[27] P. Lampen-Kelley, L. Janssen, E. C. Andrade, S. Rachel, J.-Q. Yan, C. Balz, D. G. Mandrus, S. E. Nagler, and M. Vojta, arXiv:1807.06192.
[28] C. Wellm, J. Zeisner, A. Alfonsov, A. U. B. Wolter, M. Roslova, A. Isaeva, T. Doert, M. Vojta, B. Büchner, and V. Kataev, Phys. Rev. B **98**, 184408 (2018).

[29] Y. Kasahara, T. Ohnishi, Y. Mizukami, O. Tanaka, S. Ma, K. Sugii, N. Kurita, H. Tanaka, J. Nasu, Y. Motome *et al.*, Nature (London) **559**, 227 (2018).
[30] C. Balz, P. Lampen-Kelley, A. Banerjee, J. Yan, Z. Lu, X. Hu, S. M. Yadav, Y. Takano, Y. Liu, D. A. Tennant *et al.*, Phys. Rev. B **100**, 060405 (2019).
[31] J. Knolle, G.-W. Chern, D. L. Kovrizhin, R. Moessner, and N. B. Perkins, Phys. Rev. Lett. **113**, 187201 (2014).
[32] J. Nasu, J. Knolle, D. L. Kovrizhin, Y. Motome, and R. Moessner, Nat. Phys. **12**, 912 (2016).
[33] S. Widmann, V. Tsurkan, D. A. Prishchenko, V. G. Mazurenko, A. A. Tsirlin, and A. Loidl, Phys. Rev. B **99**, 094415 (2019).
[34] S. Reschke, F. Mayr, S. Widmann, H.-A. K. von Nidda, V. Tsurkan, M. V. Eremin, S.-H. Do, K.-Y. Choi, Z. Wang, and A. Loidl, J. Phys.: Condens. Matter **30**, 475604 (2018).
[35] A. Glamazda, P. Lemmens, S.-H. Do, Y. S. Kwon, and K.-Y. Choi, Phys. Rev. B **95**, 174429 (2017).
[36] A. Little, L. Wu, P. Lampen-Kelley, A. Banerjee, S. Patankar, D. Rees, C. A. Bridges, J.-Q. Yan, D. Mandrus, S. E. Nagler *et al.*, Phys. Rev. Lett. **119**, 227201 (2017).
[37] L. Y. Shi, Y. Q. Liu, T. Lin, M. Y. Zhang, S. J. Zhang, L. Wang, Y. G. Shi, T. Dong, and N. L. Wang, Phys. Rev. B **98**, 094414 (2018).
[38] L. Wu, A. Little, E. E. Aldape, D. Rees, E. Thewalt, P. Lampen-Kelley, A. Banerjee, C. A. Bridges, J.-Q. Yan, D. Boone *et al.*, Phys. Rev. B **98**, 094425 (2018).
[39] P. A. Fleury and R. Loudon, Phys. Rev. **166**, 514 (1968).
[40] H. Gretarsson, N. H. Sung, M. Höppner, B. J. Kim, B. Keimer, and M. Le Tacon, Phys. Rev. Lett. **116**, 136401 (2016).
[41] See Supplemental Material at http://link.aps.org/supplemental/10.1103/PhysRevB.101.140410 for a theoretical analysis of the Raman and terahertz scattering mechanisms and details on the exact diagonalization calculations.
[42] J. Chaloupka and G. Khaliullin, Phys. Rev. B **94**, 064435 (2016).
[43] R. Yadav, N. A. Bogdanov, V. M. Katukuri, S. Nishimoto, J. van den Brink, and L. Hozoi, Sci. Rep. **6**, 37925 (2016).
[44] L. Janssen, E. C. Andrade, and M. Vojta, Phys. Rev. B **96**, 064430 (2017).
[45] K. Riedl, Y. Li, S. M. Winter, and R. Valentí, Phys. Rev. Lett. **122**, 197202 (2019).
[46] S. V. Vonsovskii, *Ferromagnetic Resonance: The Phenomenon of Resonant Absorption of a High-Frequency Magnetic Field in Ferromagnetic Substances* (Pergamon, Oxford, 1966).
[47] S. M. Winter, Y. Li, H. O. Jeschke, and R. Valentí, Phys. Rev. B **93**, 214431 (2016).
[48] H.-S. Kim and H.-Y. Kee, Phys. Rev. B **93**, 155143 (2016).
[49] W. Wang, Z.-Y. Dong, S.-L. Yu, and J.-X. Li, Phys. Rev. B **96**, 115103 (2017).
[50] Y. S. Hou, H. J. Xiang, and X. G. Gong, Phys. Rev. B **96**, 054410 (2017).
[51] H. B. Cao, A. Banerjee, J.-Q. Yan, C. A. Bridges, M. D. Lumsden, D. G. Mandrus, D. A. Tennant, B. C. Chakoumakos, and S. E. Nagler, Phys. Rev. B **93**, 134423 (2016).
[52] D. Wulferding, Y. Choi, S. Do *et al.*, Nat. Commun. **11**, 1603 (2020).